Preliminary Investigation of the Tensile and Compressive Material Properties of Pelvis Cortical Bone Guided by Microstructural Imaging

Devon L. Albert, Randee L. Hunter, Zachary A. Haverfield, Amanda M. Agnew

Abstract The purpose of this study was to develop methodology for quantifying the tensile and compressive material properties of human pelvis cortical bone in alignment with the regional osteon orientation. Microcomputed tomography scans were performed on the ilium, ischium, and superior pubic ramus from three pelves to quantify the osteon orientation in each region. Then, cortical bone coupons were fabricated from each of these regions, including both the anterior and posterior cortices of the ilium, from six pelves in the direction of the estimated osteon orientation. Coupons were tested in uniaxial tension and compression, and the tensile and compressive material properties were quantified. Post-test imaging of the tensile coupons was used to confirm the osteon orientation within each specimen. Differences in material properties were observed between regions with the posterior ilium typically resulting in the greatest modulus and ultimate stress and the ischium resulting in the least. Significant differences were also observed between loading modes with most regions having a greater modulus in tension, but greater ultimate stress and strain in compression. Post-test imaging revealed variability of osteon orientation within a small region of bone, resulting in coupons that were not always aligned with the osteon orientation. Future work is needed with more detailed imaging and a larger sample size to obtain more representative material properties for human pelvic cortical bone.

Keywords Ilium, Ischium, MicroCT, Osteon, Pubic ramus.

I. INTRODUCTION

Road traffic incidents and motor vehicle crashes are currently a common cause of pelvis fracture [1-6]. A study on work-related pelvic and acetabular fractures in Germany reported that such injuries, which occurred in the work-place, during a commute, or during work-related travel, commonly result in significant socioeconomic costs [5]. These costs stem from multiple months away from work, reduced earning capacity, and high long-term follow-up costs.

Advancements in autonomous driving technologies and advanced driver assistance systems (ADAS) are expected to alter the loading environment of the pelvis, which could lead to greater injury rates if not thoroughly investigated. A greater prevalence of reclined seating and removal of alternate load paths, such as the knee bolster, are possible outcomes of a shift in occupant compartment design toward comfort and away from the task of driving. These changes incentivise lap belt systems that increase the load to the pelvis in order to effectively restrain the occupant and reduce the risk of submarining. However, increased load on the pelvis can increase the risk of pelvis fracture. Therefore, new restraint system designs must balance the risk of fracture with the need to properly restrain the occupant and prevent submarining [7-9]. Furthermore, studies on how crash configurations can change with the increased adoption of ADAS using United States and German crash data project an increased proportion of intersection crashes and a decrease in more linear crash modes such as rear-end collisions [10][11]. Intersection crashes encompass a variety of potentially complex loading scenarios, which can translate to load on the pelvis from the lap belt, the door, and other interior structures.

Human Body Models (HBMs) will be important tools in evaluating new safety systems for multiple, complex loading scenarios when it is not cost-effective to perform physical tests. However, HBMs rely upon accurate

D. L. Albert (e-mail: devonalb@umich.edu; tel: +1 734-764-6504) was a Research Assistant Professor at Virginia Tech in Blacksburg, VA, USA at the time this work was performed. R. L. Hunter, Z. A. Haverfield, and A. M. Agnew are affiliated with the Injury Biomechanics Research Center at the Ohio State University in Columbus, OH, USA.

material properties to correctly predict injury risk. Brynskog *et al.* [12] demonstrated the effect of material properties on model response for the pelvis, in particular, by conducting a sensitivity analysis of the effects of different pelvis shapes, cortical bone stiffnesses, cortical bone thicknesses, and trabecular bone densities on the model's response. It was observed that cortical bone stiffness accounted for a large amount of the variation in the model response, approximately equal to that of the contributions of all of the shape parameters. Therefore, inaccurate material properties can have a large impact on the model response, potentially leading to inaccurate injury prediction.

Few studies have quantified the material properties of human pelvic cortical bone. Two studies performed three-point bending tests of cortical bone from the iliac crest, ischial ramus, and inferior pubic ramus [13][14]. Estimates of the elastic modulus were calculated using beam theory, which has limitations when applied to biological tissue. Kemper *et al.* [15] quantified the tensile material properties of cortical bone from the ilium, ischium, and superior pubic ramus of a small sample of subjects. For the ilium, the bone was tested in two different orientations, which resulted in different material properties. It was hypothesised that this was a result of the coupons having different orientations with respect to the direction of the osteons since studies on cortical bone from other regions have demonstrated a relationship between material properties and osteon direction [16].

The pelvis has a complex shape composed of multiple regions. The orientation of the osteons in pelvic cortical bone is unknown and might change throughout the different regions. There are currently no material property data for pelvis cortical bone with a known alignment with respect to the osteon direction. Furthermore, previous data have been limited to the tensile material properties of human cortical bone with no data in compression. Therefore, the purpose of this study was to develop methodology for quantifying the tensile and compressive material properties of human pelvis cortical bone from the anterior ilium, posterior ilium, ischium, and super pubic ramus in alignment with the regional osteon orientation.

II. METHODS

Seven pelves were ethically obtained for this study via the Ohio State University Body Donor Program (Table I). Six pelves were from female donors aged 58-90 years of age. Three of these pelves and one pelvis from a male donor (age: 26 years) underwent pre-fabrication imaging to quantify the orientation of the osteons within the pelves. After imaging, the right os coxa from each female pelvis was used to fabricate compression and tension coupons for material testing. The coupons were aligned with the osteon orientations quantified during pre-fabrication imaging. The tension coupons were imaged after testing to confirm the osteon orientation of each specimen. All procedures focused on four regions of interest within the pelvis: the anteromedial cortex of the ilium (anterior ilium); the posterolateral cortex of the ilium (posterior ilium); the medial cortex of the body of the ischium; and the superior pubic ramus (SPR). Further details for each step are described below.

TABLE I
DONOR CHARACTERISTICS OF PELVES USED FOR IMAGING AND MATERIAL PROPERTY TESTING

Pelvis ID	Sex	Age (years)	Height (cm)	Mass (kg)	Pre-fabrication Imaging	Material Property Testing
A	M	26	183	77.6	x	
1	F	80	161	66.9	x	x
2	F	90	160	51.3	x	x
3	F	58	168	76.4		x
4	F	59	168	61.0		x
5	F	59	166	63.7		x
6	F	68	166	53.1	x	x

Pre-Fabrication Imaging

A simplified, time-efficient pre-fabrication imaging scheme was implemented to determine whether osteon orientation could be calculated with sufficient accuracy to warrant replication on a larger scale. Pre-fabrication imaging was performed via micro-computed tomography (microCT) on four pelves (Pelvis ID: A, 1, 2, and 6) to quantify an approximate osteon orientation for the four regions of interest. Among the four pelves, at least two microCT scans were performed on each region of interest (Table II). All microCT scans were performed using a Thermo Scientific HeliScan microCT machine using operating parameters of 100 kVp and 50 mA. The resolution of each scan varied and was optimised per sample due to the varying geometry of each sample (Table II). Scans were taken of sections of the left os coxa for each pelvis. The pelves were sectioned to isolate the SPR, ischium, and/or ilium as applicable. For the ischium, sections of the body of the ischium were isolated. For the ilium, sections were generally taken from the middle of the wing medial-laterally. For pelvis 2, two sections were taken from the middle of the ilium with one located more medially (closer to the spine) and one more laterally (closer to the ASIS). All ilium sections contained both the anterior and posterior cortices. After scanning, bone-background segmentation was performed using Otsu thresholding and any noise was removed using island processing.

TABLE II
SUMMARY OF PRE-FABRICATION MICROCT SCANS

Pelvis ID	Scan Location	Resolution (µm)
A	Ilium	8.534
A	SPR	15.977
1	SPR	9.044
2	Ilium (Lateral)	11.532
2	Ilium (Medial)	9.937
2	SPR	10.092
2	Ischium	10.474
6	Ischium	9.915

A reference line was added to the 3D reconstruction of each CT scan. This line was used as a reference for the osteon orientation that could be translated from the scans to the physical pelves during coupon fabrication. For the SPR, the reference line was oriented along the long axis. For the ischium, the reference line was approximately perpendicular to the long axis of the ischial ramus and parallel to the cut made to section ischium body from the ischial ramus. For the ilium sections, the reference line was approximately perpendicular to the cut made to section the ilium from the rest of the os coxa. Representations of the reference lines, cut lines, and scanned regions are shown in Fig. 1 (*left*).

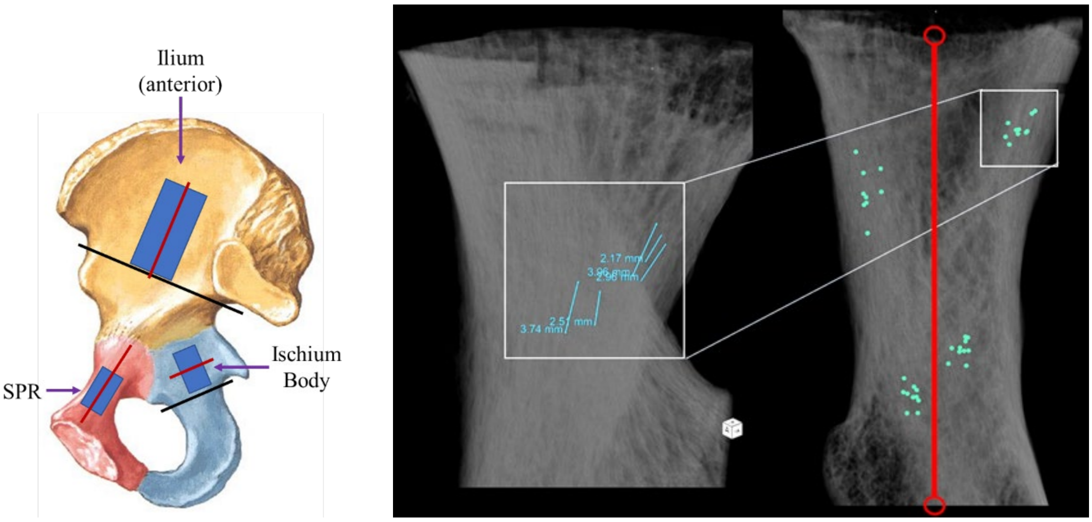

Fig. 1. *Left*: Os coxa showing approximate locations of scanned sections (blue rectangles) with reference lines (red lines) and sectioning cuts (black lines). *Right*: Exemplar 3D reconstruction of an SPR microCT scan showing the beginning and end points of the tracked pores (green), the lines representing the pores (blue), and the reference line (red).

Using the CT scans from each section, Haversian canals (pores) were tracked as a proxy for osteon orientation. The beginning and end points of 20 approximately linear pores were tracked for each section (Fig. 1, *right*). For the ischium, all 20 pores were tracked in the anterior cortex. For the ilium and SPR, 10 pores were tracked in the anterior and posterior cortices, each. The line connecting the beginning and end points of each pore represented the approximate orientation of the pore. The pore orientation and reference line were then projected into the 2-D plane representing the cortex as a surface. In other words, any angulation of the pore through the depth of the cortex was eliminated. Due to the cylindrical nature of the SPR, two approximately orthogonal planes containing the reference line were used. The 2D angle between the pore and the reference line was calculated for each pore. The aggregate angle for each region across sections and specimens was used to guide coupon fabrication.

Coupon Fabrication and Material Testing

The six right os coxae allocated for coupon fabrication were kept frozen in saline-soaked gauze until the fabrication process began. Then, the os coxae were thawed and the surrounding soft tissue was removed from the cortical surfaces of the regions of interest. The ilium, ischium, and SPR were isolated using an oscillating autopsy saw. The cut lines and reference lines shown in Fig. 1 were used as a guide so that the aggregate pore orientation calculated from the CT scans could be mapped onto each region. Specifically, the same cuts were used to isolate the ilium and ischium body during the sample fabrication process as the CT sample preparation process. These lines were used as a reference to determine sample orientation during fabrication of the tension and compression coupons. For the SPR, the osteons were perpendicular to the long axis of the structure, so no particular cut line was needed to serve as a point of reference between the CT scans and the physical structure.

Areas within each region of interest where the cortical bone was at least 1.3 mm thick were targeted for compression coupons, and areas with minimal curvature and no macroscopic pores were targeted for tension coupons. Compression and tension coupons were fabricated and tested using the methods described in [17-19]. Briefly, cylindrical compression coupons 2 mm in height and 1 mm in diameter were milled from the cortical bone using a computer numerical controlled (CNC) mill. This was a two-step process where the cylinder and one end-face were milled so that they were orthogonal. The cylinder was then cut from the bone, and the remaining end-face was milled so that it was flat and parallel to the opposite end-face. For the tension coupons, rectangular sections of cortical bone 30-mm in length and 9-mm in width were cut from the cortical bone using a custom diamond saw. Samples were sanded to a uniform thickness using fine-grit, wet sand paper before being milled into a dog-bone shape using a CNC mill. Finally, the samples were sanded to their final thickness within a tolerance of 0.05-mm. Figure 2 shows exemplar compression and tension coupons.

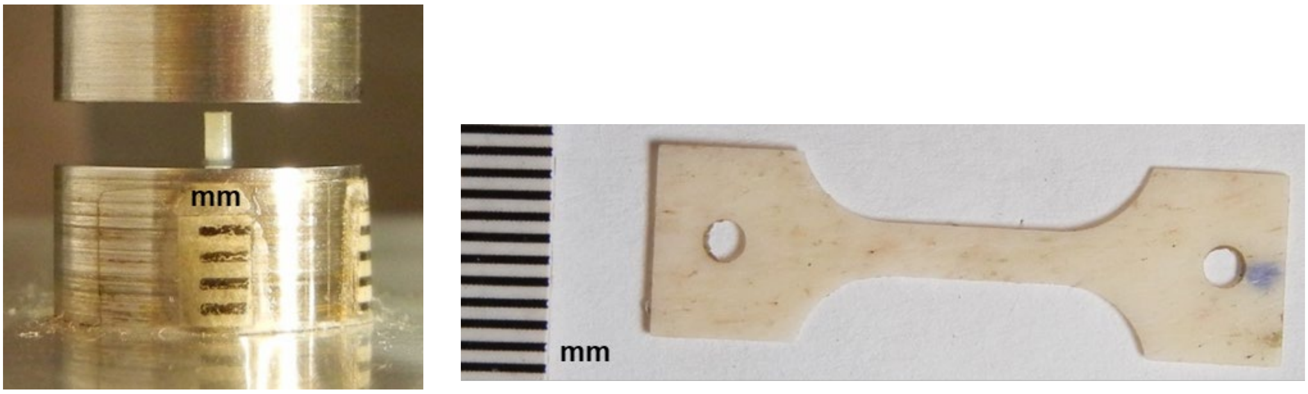

Fig. 2. *Left*: exemplar compression coupon within compression platens. *Right*: exemplar tension coupon.

All compression and tension coupons were tested to failure. Compression coupons were tested using an electric material testing machine (800LE4, Test Resources Inc., Shakopee, MN, USA) and a custom compression press with rigid loading platens (Fig. 3, *left;* Fig. 2, *left*). Compressive force was measured using a uniaxial load cell (1210ACK-300-B, Interface, Scottsdale, AZ, USA), and displacement of the specimen was measured using a deflectometer (35400-001M-ST, Epsilon Technology Corp., Jackson, WY, USA). Stress was calculated by dividing the load by the cross-section of the sample. Strain was calculated by dividing the displacement of the sample by the sample's initial height.

Tension coupons were tested using a servo-hydraulic material testing system (810, MTS Systems Corporation, Eden Prairie, MN, USA) using a custom test setup (Fig. 3, *right*). The test setup included custom grips (upper and lower) to clamp the coupon in place and a custom slack adapter, which allowed the piston to reach a constant displacement rate (velocity) prior to loading the coupon in tension. Tensile force was measured using a uniaxial reaction load cell (1500ASK-100, Interface, Scottsdale, AZ, USA). Deflection of the gage length of the coupon was measured using an extensometer (532.13F-20, MTS Systems Corporation, Eden Prairie, MN, USA) attached to the gage length of the coupon using orthodontic rubber bands. Stress was calculated by dividing the force by the cross-sectional area of the gage length. Strain was calculated by dividing the deflection of the sample by the initial distance between the extensometer blades.

For both types of coupon, the target loading rate was 0.5 strain/s. All data were collected at a rate of 20 kHz. Tension data were filtered using an SAE J211 low-pass filter with a channel frequency class (CFC) of 180 [20]. Compression data were filtered using the same filter with a pseudo-CFC of 30. Material properties were quantified from the stress-strain responses of the tension and compression coupons using the same methodology. The elastic modulus was defined as the slope of the linear region of the stress-strain curve. The yield point was quantified as the intersection of the stress-strain curve with a straight line that was offset by 0.1% strain from the linear region of the curve. The ultimate point was defined as the peak stress before failure. For both types of coupons, this corresponded to the last data point before failure. Failure for the tension coupons was clearly marked by a sudden, drastic decrease in stress. The compression coupons were able to continue sustaining load beyond the point of failure, so failure was defined as the first decrease in stress observed during the test. The total strain energy density (TSED) was calculated as the area under the stress-strain curve up until the ultimate point. The TSED was further divided into the elastic strain energy density (ESED), which was the strain energy density until the yield point, and the plastic strain energy density (PSED), which was the strain energy density between the yield and ultimate points. If multiple successful tests were performed within a region of interest for a single pelvis, the material properties from those tests were averaged before performing additional analyses.

Differences in material properties across regions of interest within each loading mode were evaluated using a one-factor ANOVA. A post-hoc Tukey's Honestly Significant Difference (HSD) test was used to determine which pairs of regions had significant differences. Then, differences in material properties between tension and compression were evaluated within each region of interest using t-tests. For all statistical analyses, the threshold for significance was a p-value less than 0.05.

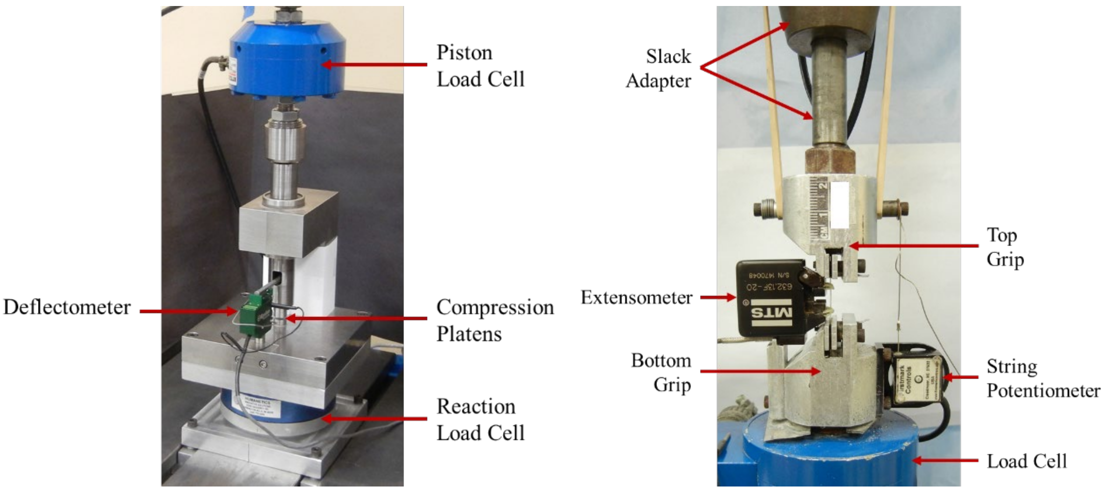

Fig. 3. Labelled test setup for compression (*left*) and tension (*right*).

Post-Test Imaging

Post-test imaging was performed on all tension coupons to qualitatively determine the true osteon orientation of the gage length of the coupons. After being tested to failure, the coupons were rinsed of any remaining intrinsic fluid with saline and dried flat. Coupons were then temporarily submerged in Xylene for clear visualisation and imaged without permanent mounting. Bright field microscopy was performed using transmitted light on a VS120 slide scanner at four times objective magnification with automatic focus. These images allowed for qualitative determination of Haversian system orientation by visualising the pores. Three categories were used to group osteon orientation into aligned (longitudinal), oblique, and transverse with respect to the gage length.

III. RESULTS

Pre-fabrication Imaging

The osteon pore orientations varied across the different regions of interest. For the SPR, the average and median pore orientations within each pelvis were within 10 degrees of the reference line (Fig. 4, *left*). Specifically, the average angle across all specimens was -4.3 degrees. Pelvis A had more variation in pore angle compared to Pelves 1 and 2 due to the SPR flaring and widening when approaching the ilium. Visual inspection indicated that the pores in this region were still aligned with the long axis of the SPR. Based on these results, it was assumed that the osteon orientation was aligned with the long axis of the SPR during coupon fabrication.

For the ischium, the average and median pore orientations were within 10 degrees of the reference line for both pelves (Fig. 4, *right*). While Pelvis 6 had a larger variation in angles, this was not localised to a particular region and might be the result of general variation in osteon orientation within this ischium sample. The average angle across all specimens was 7.5 degrees. This was within the amount of error expected from the cutting and fabrication processes. Since the pores were generally aligned with the reference line, the assumed osteon orientation was parallel to the cut line dividing the body of the ischium and the ischial ramus (Fig. 1, *left*), perpendicular to the long axis of the ischial ramus.

The average and median pore orientations for the anterior ilium were between approximately 60 and 82 degrees from the reference line, pointing slightly superior (relative to the cut line separating the iliac wing from the rest of the os coxa) and lateral (Fig. 5). The different sections within Pelvis 2 had similar pore orientations and were largely between 60 and 70 degrees. Pelvis A had greater variation in pore angle with the average being closer to 80 degrees. The average orientation across all specimens was 71.9 degrees, which was rounded to an even 70 degrees. Therefore, the assumed osteon orientation and target for fabricating the coupons was 70 degrees from the reference line or 30 degrees from the cut line.

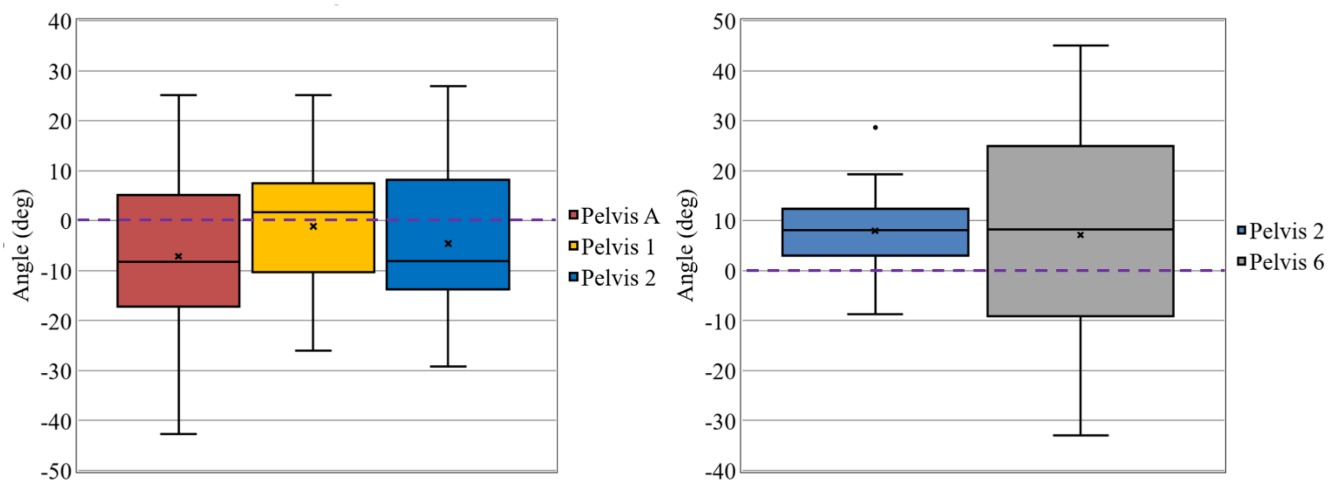

Fig. 4. Box and whisker plots depicting pore angle with respect to the reference line within each pelvis for the SPR (*left*) and ischium (*right*). Dashed lines indicate the target coupon orientation.

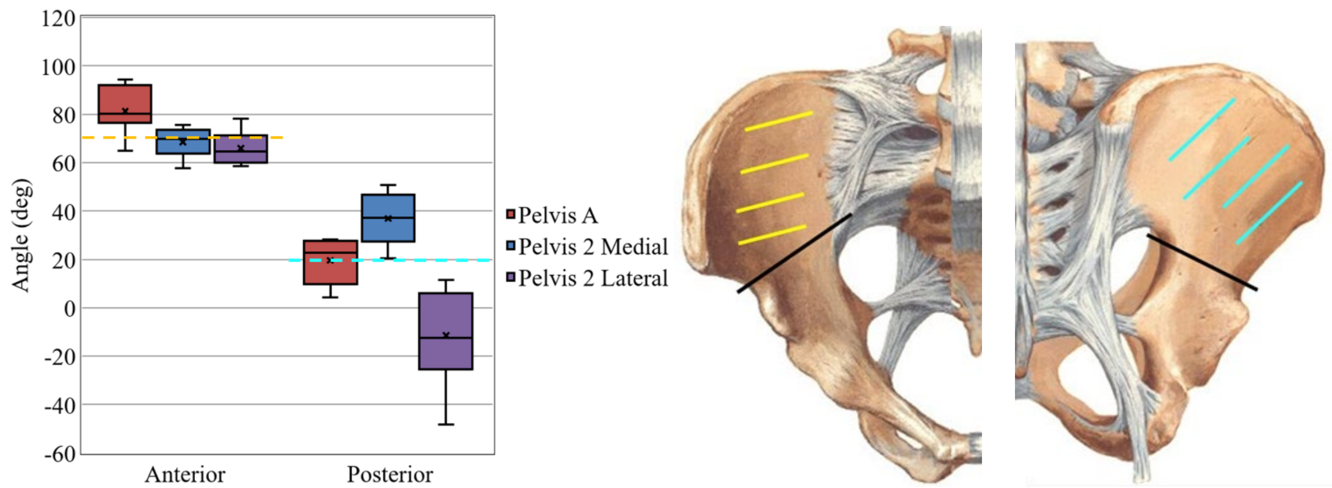

Fig. 5. *Left*: box and whisker plots depicting pore angle with respect to the reference line within each pelvis for the anterior and posterior ilium. Dashed lines indicate the target coupon orientation. *Right*: representation of the assumed osteon orientations for the anterior (yellow lines) and posterior (cyan lines) ilium. The black line represents the cut line isolating the ilium from the rest of the os coxa, which would be perpendicular to the reference line.

The average and median pore orientations for the posterior ilium were variable between pelves and regions (Fig. 5). The pores in the medial section of Pelvis 2 were largely 20-50 degrees from the reference line, pointing superior and lateral. The pores in the lateral section of Pelvis 2 showed a large variance, with an average of 2 degrees from the reference line in the inferior part of the specimen and -25 degrees in the superior part of the specimen. The pore angles observed in Pelvis A were orientated between those of the medial and lateral sections of Pelvis 2, oriented largely between 0 and 30 degrees of the reference line. It was hypothesised that the large variation in pore angle observed in the posterior ilium could be the result of local changes due to large muscle attachments. Furthermore, the pores with the most variation and most negative angles in the lateral section of Pelvis 2 were close to the iliac crest. The average angle across all scanned sections was 15 degrees. This was rounded to 20 degrees to be more consistent with the pores that were not close to the iliac crest as the crest would be removed prior to coupon fabrication. Therefore, the assumed osteon orientation and target for fabrication was 20 degrees from the reference line (70 degrees from the cut line), pointing superiorly and laterally.

Material Properties

Fifty-four successful tests were included in the final dataset across both loading modes (Table III). The average compressive and tensile material properties for each region are provided in the Appendix in Tables AI and AII. Material properties were significantly different between pelvis regions for both loading modes. In tension, all material properties, except for yield strain, exhibited significant differences between regions (Table IV, Figure 6). Most notably, the ischium frequently had lesser tensile material properties than the other regions of interest. This can be observed qualitatively in the stress-strain curves (Fig. 7). There was more overlap in the stress-strain responses of the posterior ilium, anterior ilium, and SPR. Though, the statistical analysis indicated that the posterior ilium had a significantly greater modulus, yield stress, ultimate stress, and ESED than the anterior ilium. Additionally, the SPR had a significantly greater ultimate stress, ultimate strain, and TSED than the anterior ilium.

TABLE III
FINAL TEST MATRIX INDICATING NUMBER OF SUCCESSFUL TESTS FOR EACH PELVIS, REGION OF INTEREST, AND LOADING MODE

Pelvis	Ant. Ilium		Post. Ilium		Ischium		SPR	
ID	T	C	T	C	T	C	T	C
1	1	1	1	2	2	1	1	1
2	1	2	0	1	1	1	1	1
3	1	1	1	2	1	1	1	2
4	1	2	0	1	1	2	1	1
5	1	2	1	2	0	1	1	2
6	1	1	1	2	1	1	0	0

TABLE IV
P-VALUES FOR THE ANOVAS EVALUATING DIFFERENCES BETWEEN REGIONS OF INTEREST AND T-TESTS EVALUATING DIFFERENCES BETWEEN LOADING MODES; BOLD VALUES INDICATE STATISTICAL SIGNIFICANCE

Material Property	Compression ANOVA Region of Interest	Tension ANOVA Region of Interest	Ant. Ilium t-test Loading Mode	Post. Ilium t-test Loading Mode	Ischium t-test Loading Mode	SPR t-test Loading Mode
Modulus	**0.0039**	**<0.0001**	**0.0028**	**0.0007**	0.4326	**0.0002**
Yield Stress	**0.0072**	**<0.0001**	0.4610	0.8673	**0.0056**	0.3784
Yield Strain	0.4264	0.0541	**0.0006**	**<0.0001**	**<0.0001**	**0.0007**
Ultimate Stress	**0.0150**	**<0.0001**	**0.0192**	0.5269	**0.0004**	0.2404
Ultimate Strain	**0.0012**	**0.0129**	**0.0003**	**0.0010**	**<0.0001**	**0.0118**
ESED	0.0767	**0.0008**	**0.0079**	**0.0130**	**0.0033**	0.1299
PSED	**0.0169**	**0.0211**	**0.0055**	**0.0376**	**<0.0001**	0.3332
TSED	0.0526	**0.0035**	**0.0005**	**0.0234**	**<0.0001**	0.2398

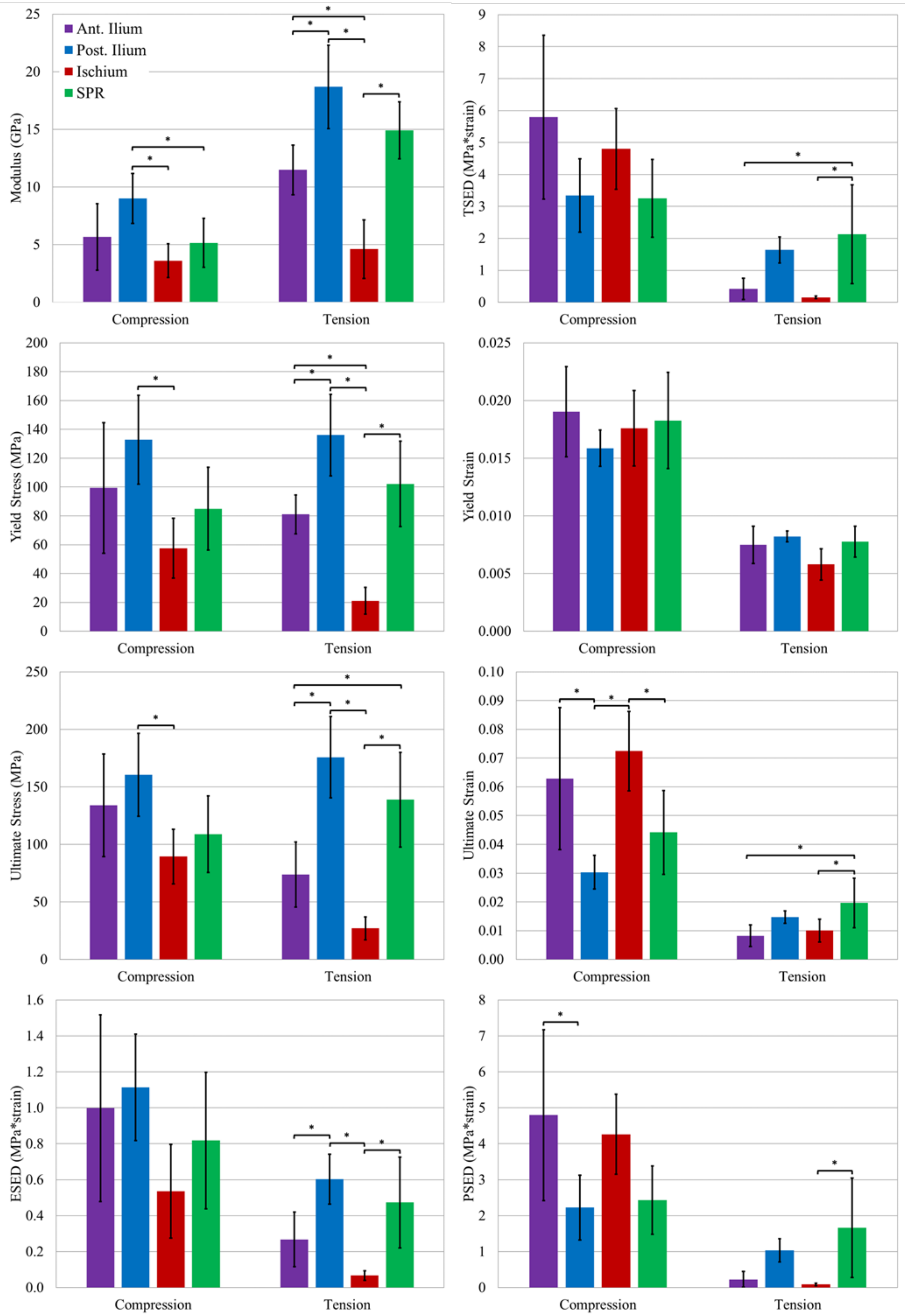

Fig. 6. The average and standard deviation material properties for each region of interest and each loading mode. Brackets with an asterisk indicate the material properties of the two regions indicated are significantly different via the Tukey's HSD test.

There were fewer significant differences between pelvis regions for the compressive material properties. These included the modulus, yield stress, yield strain, ultimate stress, ultimate strain, and PSED (Table IV, Fig. 6). The Tukey's HSD test indicated that both the anterior ilium and the ischium had significantly greater ultimate strains than the posterior ilium. The ultimate strain for the ischium was also greater than that of the SPR. The posterior ilium had a significantly greater modulus, yield stress, and ultimate stress than the ischium.

Significant differences between material properties in tension and compression varied by region within the pelvis. The ischium had the most material properties that significantly altered with loading mode, while the SPR had the least. For the ischium, all compressive material properties were significantly greater than the tensile material properties except for the modulus, which was not significantly different between the two loading modes. For the anterior and posterior ilium, all material properties were significantly different between loading modes apart from the yield stress, which was not significantly different for both regions, and the ultimate stress, which was not significantly different for the posterior ilium. All material properties with significant differences were greater in compression except for the modulus, which was greater in tension. The SPR had the least amount of material properties with significant differences between compression and tension. For the SPR, the modulus was significantly greater in tension, while the yield strain and ultimate strain were greater in compression.

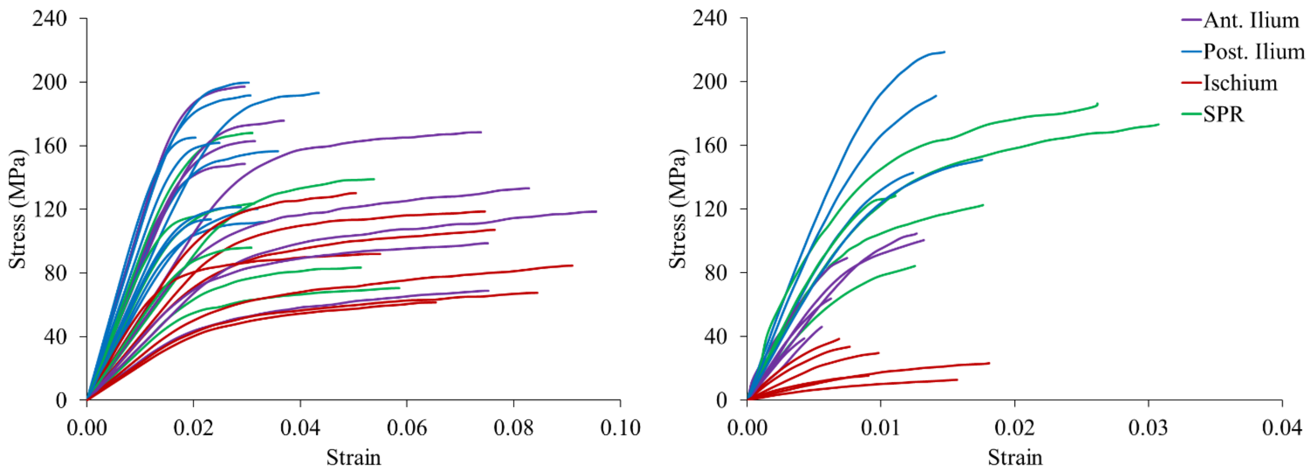

Fig. 7. Compressive (*left*) and tensile (*right*) stress-strain curves for all regions and pelves.

Post-test Imaging

The qualitative alignment of osteons was assessed for 20 of the 21 tension coupons after failure. For one of the coupons, the osteon alignment relative to the gage length was not able to be determined. Exemplar coupons with aligned (longitudinal), oblique, and transverse osteon orientations are provided in Fig. 8(a)-(c). Osteon orientation sometimes varied within a coupon and within the gage length (Fig. 8(d)). In these cases, the osteon orientation closest to the location of failure was recorded. The number of coupons aligned with the osteon direction varied with pelvis region (Fig. 9). The SPR had the best alignment, with all coupons aligned with the osteon direction. For the posterior ilium, half of the coupons were aligned and half were oblique. For the anterior ilium, two coupons were aligned, three coupons were oblique, and one coupon was transverse. The ischium was the least aligned with the osteon direction. Of the five ischium coupons with known alignments, one was oblique and four were transverse. No ischium coupons were longitudinally aligned.

IV. DISCUSSION

The material properties observed during this study were comparable to those observed in previous studies on pelvic cortical bone. Kuhn *et al.* [14] tested beams of iliac crest cortical bone from two male subjects in three-point bending. The average elastic moduli from the 63-year-old and 23-year-old subjects were 5.26 ± 2.09 GPa and 3.76 ± 1.68 GPa, respectively. Gebhardt *et al.* [13] tested cortical bone from the ischial ramus and inferior pubic ramus in three-point bending and reported an average elastic modulus of 1.45 GPa. Both of these studies relied upon beam theory equations to estimate the material properties. However, Kemper *et al.* [15] tested cortical bone from the anterior ilium, posterior ilium, ischial body, and SPR in tension, which is more comparable to the current study in terms of methodology and pelvis regions. The average elastic modulus for the different regions of interest ranged from 8.6 to 12.6 GPa. In the current study, the average tensile elastic modulus for the different regions of interest ranged from 4.6 to 18.7 GPa. The current study also showed a wider range of values for tensile ultimate stress compared to [15]. For ultimate stress, average values across for each region ranged from 27. 0 to 175.8 GPa and from 45.2 to 121.1 GPa for the current study and [15], respectively. Conversely, [15] reported a greater range of tensile ultimate strain values (0.007 to 0.030) compared to the current study (0.008 to 0.020).

Fig. 8. Exemplar tension coupons with (a) longitudinal, (b) oblique, (c) transverse, and (d) varying osteon alignment with respect to the gage length.

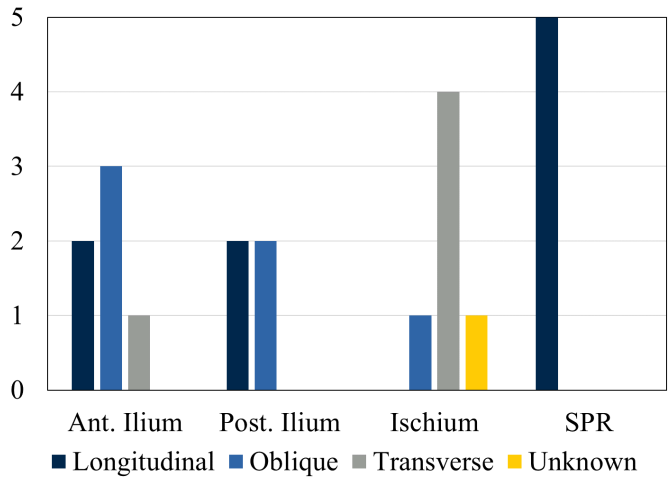

Fig. 9. Number of tension coupons within each pelvis region that had longitudinal, oblique, transverse, and unknown alignment with respect to the osteon direction within the gage length.

Though the current study and [15] investigated the same regions of the pelvis, the alignment of the tension coupons within a region was not always the same between the two studies. For example, the ischium coupons in [15] were fabricated in an approximately vertical orientation, aligned with the long axis of the ischial body and approximately perpendicular to the SPR. In the current study, the ischium coupons were perpendicular to the long axis of the ischial ramus. Effectively, this difference produces coupons that are approximately 45-90 degrees different in alignment between the two studies. Post-test imaging of the tension coupons revealed that the ischium coupons from the current study were typically transverse to the osteon orientation, indicating that the coupons from [15] were likely more aligned with the osteon orientation. This orientation difference aligns with the lower tensile modulus, ultimate stress, and ultimate strain observed in the current study relative to [15] (Table AIII), as material properties are known to be greater in the direction of the osteons [16]. For both the current study and [15], the tension coupons from the SPR were aligned with the long axis of the structure and the direction of the osteons. As a result, observed tensile moduli, ultimate stresses, and ultimate strains were similar between the two studies for the SPR.

For the anterior and posterior ilium, [15] fabricated coupons in two directions: vertical, which was approximately parallel to the spine; and horizontal, which was perpendicular to vertical. The anterior ilium coupons in the current study had a similar alignment to the horizontal coupons from [15]. Therefore, similar tensile moduli were observed in the two studies for anterior ilium coupons with this alignment. However, [15] reported greater ultimate stresses and strains compared to the current study. Variation in bone quality between the subjects in the two studies could be contributing to these material property differences. The vertical coupons from the anterior ilium in [15] resulted in decreased material properties relative to the horizontal coupons in both studies. The current study showed that the osteon direction within the anterior ilium was variable, resulting in some coupons that were aligned with the osteons and some that were not. Based on the results of both studies, it is likely the approximately horizontal coupons were more aligned with the osteon direction than the vertical coupons. The posterior ilium coupons in the current study were fabricated at an angle that was between the horizontal and vertical coupons from [15], resulting in a coupon alignment that could be called diagonal with respect to the horizontal and vertical axes. These diagonal coupons had greater elastic moduli, ultimate stresses, and ultimate strains compared to the horizontal and vertical coupons from [15], which had approximately equal material properties. Post-test imaging diagonal coupons were either aligned or obliquely aligned with the osteon direction. Despite variation in osteon alignment within the posterior ilium, the diagonal coupons were likely more aligned with the osteon direction than the vertical or horizontal coupons.

Statistical differences between tensile and compressive material properties were observed in this study, but no compressive material property data were available in the literature for human pelvis cortical bone to assess the results observed in this study. Previous studies on human cortical bone from other regions reported differences between tensile and compressive material properties. For human rib cortical bone, the modulus, yield stress, yield strain, ultimate stress, ESED, PSED, and TSED were all significantly different between tension and compression [18]. The tensile modulus and PSED were significantly greater than the compressive modulus, while the remaining material properties were significantly greater in compression. This partially aligns with the current study's results in the pelvis, where the modulus was significantly greater in tension, but the remaining properties, when significantly different, were greater in compression. Other studies investigating human femoral and tibial cortical bone have also observed greater ultimate stresses in compression compared to tension [21][22].

Compressive ultimate strain was significantly greater than the tensile ultimate strain for all pelvis regions in the current study. However, previous studies on human rib cortical bone [18] and human femoral cortical bone [22] did not observe significant differences between compressive and tensile ultimate strain. It can be difficult to define an ultimate point during compression testing since the material continues to withstand force after failure. For this study, the tensile and compressive ultimate points were both defined as the last point before a decrease in stress occurred. Therefore, the definition of the ultimate point between the two loading modes is the same and should not bias the results. It could be possible that the microstructure of cortical bone in the pelvis, specifically, could result in a greater compressive ultimate strain. For example, some of the ischium and SPR samples tested by Kemper *et al.* [15] in tension experienced ultimate strains comparable to those observed for these structures in compression in the current study. It is also possible that osteon alignment affects material properties differently in tension and compression. A study using bovine femoral bone found that coupons transverse to the osteon direction experienced a more brittle failure, undergoing less strain than their counter parts that were longitudinal [23]. However, this effect was less prominent in compression. So, osteon alignment might have a greater influence on tensile ultimate strain compared to compressive ultimate strain, contributing to differences between loading modes observed in the current study.

While the tension and compression coupons were oriented in the same direction within each pelvis region, they did not necessarily have the same osteon orientation. Marked variability in osteon orientation was sometimes observed across the 30 mm long tension coupons per the post-test imaging (Fig. 8(d)). Though compression coupons were generally fabricated from areas close to the tension coupons, this variability could result in tension and compression coupons from the same region with different osteon orientations. Furthermore, the small size of the compression coupons (1 mm in diameter and 2 mm in height) makes them more sensitive to local changes in osteon orientation. The dimensions of the coupons were limited by the thickness and geometry of the cortical bone in the pelvis, so larger dimensions were not feasible. It was not possible to obtain post-test imaging of the compression coupons due to their geometry and sustained damage. So, it cannot be assumed that the compression coupons have the same osteon orientation as the tension coupons. Therefore, differences in osteon orientation could also be affecting the observed differences between tensile and compressive material properties.

A previous study systematically examined the effect of osteon orientation on tensile and compressive material properties in human and bovine femoral cortical bone by testing coupons that were aligned with, transverse to, and oblique to (30 and 60 degree offsets) the osteon orientation [16]. In tension, the modulus, ultimate stress, and ultimate strain all decreased when changing from an aligned to transverse orientation. Among the oblique orientations, there was typically a large decrease in material properties when changing from 30 to 60 degrees oblique, with the 60-degree orientation resulting in material properties more similar to the transverse orientation. Similar trends were observed in compression, except for the compressive ultimate strain, which did not vary much with changes in coupon orientation. The qualitative category of oblique alignment was used in the current study to describe any coupons that were not longitudinally or transversely aligned with the osteon orientation, encompassing a wide range of orientations. Depending on the actual angle between the coupon orientation and osteons, the sample could yield results more similar to an aligned sample or transverse sample, making it difficult to draw conclusions based on these samples without a more quantitative orientation. However, the variability of osteon orientation across some samples renders quantification challenging. Future work with a more systematic study could better investigate the effect of osteon orientation and its variability on observed material properties.

Post-test imaging revealed that the majority of ischium tension coupons in this study were transverse to the osteon direction. Based on the findings of previous literature that investigated the relationship between material properties and sample orientation [16][23], as well as the greater material properties reported for the ischium by Kemper et al. [15], it is likely that the ischium material properties observed in this study are lower than those that would be observed when loaded in the direction of the osteons. It is unknown why the pre-fabrication imaging used to guide the orientation of the coupons indicated a different osteon orientation than the post-test imaging. It is possible the pre-fabrication imaging was too simplistic to accurately guide fabrication efforts given the variability in osteon orientation observed in both pre-fabrication and post-test imaging. Specifically, the pre-fabrication imaging focused on narrow regions of bone and only tracked a limited number of pores. The observed variability in osteon orientation may be evidence of multi-vectored loading within the ischium. For instance, the region imaged during prefabrication may have contained osteons oriented along a dominant strain trajectory, while adjacent or slightly deeper microstructure samples may reflect a competing load direction or mixed generations of remodelling. More detailed tracking across larger areas is likely needed to more accurately assess osteon orientation and isolate dominant pore orientation.

While differences in osteon orientation are likely contributing to the regional differences in material properties observed in this study, it is possible that variation in other microstructural elements across regions are also affecting the material properties. For example, the tensile modulus and ultimate stress for the posterior ilium were greater on average than those from the SPR even though the SPR coupons were better aligned with the osteons. Therefore, there are likely other microstructural properties contributing to the differences between these two regions. These differences in material properties between regions, coupled with differences in geometry, could lead to differences in fracture risk between regions of the pelvis. This variability would be important to capture in HBMS, which are used to evaluate multiple impact directions that load different regions of the pelvis.

The material properties reported in this study should be considered preliminary. Only six pelves were tested to quantify the material properties, and all of these pelves were from older adult females. Material properties of cortical bone, particularly in tension, are known to be correlated with age [18][19][21][24][25], so this sample might not accurately represent the population as a whole. More work is needed, including a wider range of ages and other aspects of population variability, to more accurately quantify the material properties of pelvis cortical bone before implementation into HBMs meant to represent populations not present in this subject pool.

V. CONCLUSION

This study developed a methodology for fabricating and testing human pelvis cortical bone in tension and compression in the same direction as the osteons. Preliminary material property data for the anterior ilium, posterior ilium, ischium, and SPR were quantified, and this is the first study to report compressive material properties for human pelvic cortical bone. Significant differences were observed in material properties between loading modes and across pelvic regions. However, the coupons were not always aligned with the osteon direction as intended due to the degree of variability of osteon orientations within regions and limitations of the pre-fabrication imaging. Future work is needed with more detailed quantification of imaging and a larger sample size to obtain more representative material properties for human pelvic cortical bone.

VI. ACKNOWLEDGEMENTS

The authors would like to thank the anatomical donors of The Ohio State University Body Donation Program for making this research possible. The authors would also like to acknowledge the former faculty, staff, and students of the Sled Lab at Virginia Tech for their contributions to the study. Finally, the authors would like to thank the Research Consortium for Crashworthiness in Automated Driving Systems (RCCADS) for funding this study. The content of this manuscript is solely the responsibility of the authors and does not necessarily represent the official views of RCCADS or its members.

VII. REFERENCES

[1] Abdelrahman, H., El-Menyar, A., *et al*. (2020) Patterns, management, and outcomes of traumatic pelvic fracture: insights from a multicenter study. *Journal of Orthopaedic Surgery and Research*, **15**(1): p. 249.

[2] Dai, J., He, J., Ying, Y., Huang, D., Feng, L. (2023) Clinical and epidemiological characteristics of 369 patients with pelvic fractures in Eastern Zhejiang Province of China: a retrospective study. *BMC Musculoskeletal Disorders*, **24**(1): pp. 495.

[3] Efendiyeva, E., Messova, A., *et al*. (2021) Epidemiology of Pelvic Ring Fractures and Injuries: A Retrospective Study. *Open Access Macedonian Journal of Medical Sciences*, **9**(A): pp. 901–905.

[4] Ghosh, S., Aggarwal, S., Kumar, V., Patel, S., Kumar, P. (2019) Epidemiology of pelvic fractures in adults: Our experience at a tertiary hospital. *Chinese Journal of Traumatology*, **22**(03): pp. 138–141.

[5] Hinz, N., Dehoust, J., *et al*. (2023) Epidemiology and socioeconomic consequences of work-related pelvic and acetabular fractures recorded in the German Social Accident Insurance. *Injury*, **54**(8): p. 110848.

[6] Pereira, G. J. C., Damasceno, E.R., *et al*. (2017) Epidemiology of pelvic ring fractures and injuries. *Revista Brasileira de Ortopedia (English Edition)*, **52**(3): pp. 260–269.

[7] Brynskog, E., Östh, J., Larsson, K.-J., Iraeus, J. (2025) Effect of occupant and restraint variability in reclined positions on submarining probability in frontal car crash scenarios. *Frontiers in Bioengineering and Biotechnology*, **13**: p. 1570572.

[8] Östling, M. and Eriksson, L. (2022) Simulating the Influence of Lap Belt Load Limiting on Injury Risks for Upright and Reclined Occupants with the SAFER Human Body Model. *Proceedings of the IRCOBI Conference, 2022, Porto, Portugal, Paper Number IRC-22-264*.

[9] Östling, M. and Lubbe, N. (2023) Load-limiting in the lap belt reduces injury risks associated with new seating positions. *International Journal of Crashworthiness*, **28**(5): pp. 591–600.

[10] Östling, M., Jeppsson, H., Lubbe, N. (2019) Predicting crash configurations in passenger car to passenger car crashes to guide the development of future passenger car safety. *Proceedings of the IRCOBI Conference*, 2019, Florence, Italy.

[11] Östling, M., Lubbe, N., Jeppsson, H., Puthan, P. (2019) Passenger car safety beyond ADAS: defining remaining accident configurations as future priorities. *Proceedings of the 26th International Technical Conference on the Enhanced Safety of Vehicles, 2019, Eindhoven, Netherlands*,

[12] Brynskog, E., Iraeus, J., Pipkorn, B., Davidsson, J. (2022) Population variance in pelvic response to lateral impacts-a global sensitivity analysis. *Proceedings of the IRCOBI Conference*, 2022, Porto, Portugal.

[13] Gebhardt, M., Slowik, V., Steinke, H. (2024) Drying irreversibly affects the elastic behavior of pelvic cortical bone. *Journal of the Mechanical Behavior of Biomedical Materials*, **152**: p. 106432.

[14] Kuhn, J.L., Goldstein, S.A., *et al*. (1989) Comparison of the trabecular and cortical tissue moduli from human iliac crests. *Journal of Orthopaedic Research*, **7**(6): pp. 876–884.

[15] Kemper, A.R., McNally, C., Duma, S.M. (2008) Dynamic tensile material properties of human pelvic cortical bone. *Biomedical Sciences Instrumentation*, **44**: pp. 417–418.

[16] Reilly, D.T. and Burstein, A.H. (1975) The elastic and ultimate properties of compact bone tissue. *Journal of Biomechanics*, **8**(6): pp. 393–405.

[17] Albert, D.L., Kang, Y.-S., Agnew, A.M., Kemper, A.R. (2017) A Comparison of Rib Structural and Material Properties from Matched Whole Rib Bending and Tension Coupon Tests. *Proceedings of the IRCOBI Conference*, 2017, Antwerp, Belgium.

[18] Albert, D.L., Katzenberger, M.J., Agnew, A.M., Kemper, A.R. (2021) A comparison of rib cortical bone compressive and tensile material properties: Trends with age, sex, and loading rate. *Journal of the Mechanical Behavior of Biomedical Materials*, **122**: p. 104668.

[19] Katzenberger, M.J., Albert, D.L., Agnew, A.M., Kemper, A.R. (2020) Effects of sex, age, and two loading rates on the tensile material properties of human rib cortical bone. *Journal of the Mechanical Behavior of Biomedical Materials*, **102**.

[20] SAE (2014) Instrumentation for Impact Test - Part 1 - Electronic Instrumentation, SAE International.

[21] Burstein, A.H., Reilly, D.T., Martens, M. (1976) Aging of bone tissue: mechanical properties. *Journal of Bone & Joint Surgery*, **58**(1): pp. 82–86.

[22] Reilly, D.T., Burstein, A.H., Frankel, V.H. (1974) The elastic modulus for bone. *Journal of Biomechanics*, **7**(3): pp. 271–275.

[23] Li, S., Demirci, E., Silberschmidt, V.V. (2013) Variability and anisotropy of mechanical behavior of cortical bone in tension and compression. *Journal of the Mechanical Behavior of Biomedical Materials*, **21**: pp. 109–120.

[24] Lindahl, O. and Lindgren, A.G. (1967) Cortical bone in man. II. Variation in tensile strength with age and sex. *Acta Orthopaedica Scandinavica*, **38**(2): p. 141.

[25] McCalden, R.W., McGeough, J.A., Barker, M.B. (1993) Age-related changes in the tensile properties of cortical bone. The relative importance of changes in porosity, mineralization, and microstructure. The *Journal of Bone and Joint Surgery American edition*, **75**(8): pp. 1193–1205.

VIII. APPENDIX

TABLE AI

AVERAGE COMPRESSIVE MATERIAL PROPERTIES BY REGION.

Material Property	Units	Ant. Ilium	Post. Ilium	Ischium	SPR
Modulus	GPa	5.66	9.01	3.60	5.15
Yield Stress	MPa	99.4	132.7	57.6	84.9
Yield Strain	strain	0.019	0.015	0.018	0.018
Ultimate Stress	MPa	133.9	160.5	89.5	108.9
Ultimate Strain	strain	0.063	0.030	0.072	0.044
ESED	MPa*strain	1.00	1.11	0.54	0.82
PSED	MPa*strain	4.80	2.23	4.26	2.43
TSED	MPa*strain	5.80	3.34	4.80	3.25

TABLE AII

AVERAGE TENSILE MATERIAL PROPERTIES BY REGION.

Material Property	Units	Ant. Ilium	Post. Ilium	Ischium	SPR
Modulus	GPa	11.5	18.7	4.6	14.9
Yield Stress	MPa	81.0	136.1	21.1	102.2
Yield Strain	strain	0.0075	0.0082	0.0058	0.0078
Ultimate Stress	MPa	73.8	175.8	27.0	138.8
Ultimate Strain	strain	0.0082	0.0147	0.0101	0.0196
ESED	MPa*strain	0.27	0.60	0.07	0.47
PSED	MPa*strain	0.22	1.04	0.087	1.66
TSED	MPa*strain	0.42	1.64	0.15	2.13

TABLE AIII

COMPARISON OF AVERAGE (STANDARD DEVIATION) TENSILE MATERIAL PROPERTIES FROM THE CURRENT STUDY WITH KEMPER ET AL.

Region	Source	Alignment	Modulus (GPa)	Ultimate Stress (MPa)	Ultimate Strain (strain)
Ant. Ilium	Current Study	Approximately Horizontal	11.5 (2.2)	73.8 (28.3)	0.008 (0.004)
Ant. Ilium	Kemper *et al.*	Horizontal	12.6 (0.8)	110.6 (15.4)	0.019 (0.006)
Ant. Ilium	Kemper *et al.*	Vertical	8.6 (2.0)	45.2 (10.8)	0.007 (0.002)
Post. Ilium	Current Study	Diagonal	18.7 (3.6)	175.8 (35.5)	0.015 (0.002)
Post. Ilium	Kemper *et al.*	Horizontal	11.6 (2.5)	81.1 (13.1)	0.007 (0.004)
Post. Ilium	Kemper *et al.*	Vertical	11.3 (2.1)	78.7 (21.1)	0.010 (0.003)
Ischium	Current Study	Approximately Horizontal	4.6 (2.5)	27.0 (10.0)	0.010 (0.004)
Ischium	Kemper *et al.*	Approximately Vertical	8.9 (1.4)	81.9 (32.8)	0.024 (0.020)
SPR	Current Study	Aligned with Long Axis	14.9 (2.5)	138.8 (41.2)	0.020 (0.009)
SPR	Kemper *et al.*	Aligned with Long Axis	12.5 (0.2)	121.1 (20.4)	0.030 (0.024)